LOAD-FACTOR STABILITY ANALYSIS OF EMBANKMENTS ON SATURATED SOIL DEPOSITS

By Young-Kyo Seo[1] and Colby C. Swan,[2] Member, ASCE

ABSTRACT: A continuum-based finite-element methodology is established for quantifying the stability of earthen embankments built on saturated soil deposits. Within the methodology the soil is treated as a fluid-solid porous medium, in which the soil skeleton's constitutive behavior is modeled using a smooth elastoplastic cap model that features continuous coupling between deviatoric and volumetric plasticity. In the stability analysis procedure, self-weight of the embankment soils is monotonically increased at rates characteristic of the embankment construction time, until instability mechanisms develop. The transient effects of excess pore pressures and their impact on soil strength are explicitly modeled, allowing for computation of embankment safety factors against instability as a function of construction rate. Details on the proposed method are presented and discussed, including (1) how the construction rate of an embankment can be modeled; (2) how load-based safety factors can differ from resistance-based safety factors; and (3) solved example problems corresponding to a case history of an embankment failure.

INTRODUCTION AND MOTIVATION

The objective of this work is to develop methods for stability analysis of earthen embankments constructed on saturated soil deposits. Using classical methods and assumptions, stability analysis of such systems typically proceeds using Mohr-Coulomb soil models and various slice-type methods (Nash 1987) and by assuming that the saturated soil has a response behavior that is either fully undrained (short-term response) or fully drained (long-term response). Because the computed factors of safety against instability associated with the fully drained and fully undrained soil assumptions are generally not close in value, with undrained stabilities being significantly less than drained stabilities, the classical methods can leave considerable uncertainty directly attributable to time-dependent pore-pressure diffusion effects. Methods of slope stability analysis are thus needed that take into account the rate at which the embankment is constructed together with the spatially/temporally evolving pore-pressure field it generates in the underlying soil deposit. Such stability information is often needed by engineers planning safe yet timely rates of construction for embankment systems.

When analyzing geotechnical systems, both load and resistance factors, analogous to those used in structural engineering, can be used to quantify the stability of the system. Load factors of safety against instability are simply the ratio of the load magnitude that first generates instability of the system to the magnitude of the expected load, while the strength or resistance of the system is held constant. Resistance factors of safety against instability are the ratio of actual system strength (or resistance) to reduced system strength at which system instability first occurs, while holding the loading on the system fixed. Although classical slope stability methods (such as slice methods) typically produce resistance-type safety factors, both factors are valid, although not necessarily the same. In Swan and Seo (1999), where continuum/FEM models for computing both resistance and load factors of safety against instability were presented for soil slopes, it was shown that neither

method is consistently more or less conservative than the other. In this work, load-based stability analysis is investigated for sand embankments constructed on soft, saturated clay soil deposits. Load-based stability analysis techniques are potentially attractive, because they quite naturally permit stability analysis of embankments as a function of construction time.

Geotechnical analysts who utilize load-based safety factors and load-based stability analysis should be well aware of the differences between such methods and the more traditional resistance-based factors of safety used in geotechnical engineering. In load-based stability analysis, the loading on the system is increased until it fails. In some circumstances, if unrealistic soil models are used, load-based stability analysis can yield meaningless results. For example, in the special case of very gentle slope systems (of small steepness), as the unit weight of the soil mass increases, the shear strength of the soil can increase more rapidly than the mobilized shear stresses in the soil mass. If the soil shear strength is modeled with a linear Mohr-Coulomb or linear Drucker-Prager failure envelope, the modeled shear strength continues to increase indefinitely in proportion to increased confining stresses. For cases such as these, the combination of gentle slope systems and unrealistic soil models lead to the result that no amount of increased load will generate failure of the modeled system and the predicted load-based factor of safety will be infinite.

To rectify this potential problem with load-based safety factors, analysts who use load-based stability analysis must generally use more realistic soil models. It is well recognized that no soil continues to gain shear strength indefinitely with increased confining stresses. At some point, there is a limit (or saturation) to increase of shear strength from frictional effects. The load-based safety factors and stability analysis can be guaranteed to give meaningful results only when the soil strength models used feature a realistic saturation of friction effects or an ultimate limit on the shear strength of the soil. Consequently, soil models with these characteristics are used in this work.

The essence of the load-based stability method to be presented involves constructing representative continuum finite-element models of embankment systems on saturated foundation soils that have been previously consolidated or overconsolidated. Although the self-weight loading on foundation soils is held fixed, the self-weight loading on the embankment system is monotonically increased, simulating its gradual construction up to the point at which destabilizing mechanisms fully develop. Because the proposed framework computes both time-dependent consolidation and shear failure effects, it is a generalization of preceding works [i.e., Smith and Hobbs (1976)] that have utilized multiphase continuum/

[1]Postdoctoral Assoc., Dept. of Civ. and Envir. Engrg., Univ. of Iowa, Iowa City, IA 52242. E-mail: yseo@diego.ecn.uiowa.edu

[2]Assoc. Prof., Dept. of Civ. and Envir. Engrg., Ctr. for Comp.-Aided Des., Univ. of Iowa, Iowa City, IA 52242 (corresponding author). E-mail: swan@diego.ecn.uiowa.edu

FEM models to compute consolidation settlements under embankments, without concern for possible shear failures of the system. This proposed approach is also a generalization of the embankment analysis techniques of Huang et al. (1992), because it explicitly models pore-pressure distributions and temporal diffusion effects in the foundation soils along with their effect on development of global instability mechanisms. The ratio of ultimate to actual embankment loading magnitude provides a natural load-based factor of safety for the embankment system. Because the proposed methods are embedded within a fairly standard FEM framework, they can be used with a wide variety of realistic constitutive soil models and the framework can keep track of in situ soil displacements, effective stresses, pore pressure, and related soil strengths.

So that coupled compressibility and shear failure behaviors of soils can be considered in embankment stability analysis, elastoplastic cap models are employed. Unlike classical Mohr-Coulomb models, elastoplastic cap models can take into account normal and overconsolidation effects in the foundation soils beneath the embankment. In this work, a novel, smooth, elastoplastic cap model (Swan and Seo 2000) is employed, which is a smooth variation of preceding nonsmooth cap models (Roscoe et al. 1958; Burland 1965; DiMaggio and Sandler 1971; Bathe et al. 1980; Desai et al. 1986; Simo et al. 1988; Chen and Mizuno 1990; Hofstetter et al. 1993).

Accounting for transient pore-pressure diffusion effects in embankment stability analysis requires multiphase continuum modeling capabilities, which can be achieved with a variety of classical porous medium theories (Biot 1962; Truesdell 1965). In recent years, a number of computational implementations of these porous medium theories have been developed especially for soils wherein the compressibility of soil grains is typically much smaller than that of the pore water, which is in turn much less compressible than the soil skeleton.

For simplicity, these implementations can be grouped into so-called velocity formulations (Prevost 1980, 1987) and so-called pressure formulations (Zienkiewicz and Shiomi 1984; Borja 1986; Prevost 1998). Although both the velocity and the pressure formulations have their own advantages, a porous medium treatment with a velocity formulation is used here because it leads to homogeneous systems of finite-element equations, thus circumventing the algorithmic complexities and potential instabilities associated with solving heterogeneous systems of finite-element equations for nodal velocities and pressures (Zienkiewicz et al. 1988; Farhat et al. 1991; Prevost 1998).

MULTIPHASE EMBANKMENT STABILITY ANALYSIS

Porous Medium Analysis Problem

The response of soil embankments subjected to gravitational loading will be modeled herein as a porous, granular solid skeletal continuum interacting with a continuous pore fluid. The resulting coupled parabolic field equations of linear momentum balance for the soil skeleton and the pore fluid can be written as follows (Prevost 1980):

$$\nabla \cdot (\boldsymbol{\sigma}' - n^s p_w \mathbf{1}) - \boldsymbol{\xi} \cdot (\mathbf{v}_s - \mathbf{v}_w) + \rho^s \mathbf{b} = \mathbf{0} \qquad (1)$$

$$-\nabla(n^w p_w) + \boldsymbol{\xi} \cdot (\mathbf{v}_s - \mathbf{v}_w) + \rho^w \mathbf{b} = \mathbf{0} \qquad (2)$$

where $\boldsymbol{\sigma}'$ = effective stress; p_w = pore fluid pressure; n^w and n^s = respective fluid and solid volume fractions in soil; $\mathbf{v}_w$ and $\mathbf{v}_s$ = respective velocities of the fluid and solid phases; ρ^w and ρ^s = respective mass densities of the fluid and solid phases per gross volume (that is, $\rho^s = n^s \rho_s$ and $\rho^w = n^w \rho_w$); $\boldsymbol{\xi}$ = soil's resistivity tensor, which is inversely proportional to the permeability tensor; and $\mathbf{b}$ = time- and position-dependent body force per unit mass (gravity) vector applied to the soil mass.

Introducing appropriate initial and boundary conditions, and using a Galerkin-weighted residual formulation in which the real and variational kinematic fields are expanded in terms of the same nodal basis functions, leads to the following equilibrium force balance equations at each unrestrained node A in the mesh of the soil domain, as here at the $(n + 1)$th time step

$$(\mathbf{r}_A)_{n+1} = (\mathbf{f}_A^{\text{int}})_{n+1} - (\mathbf{f}_A^{\text{ext}})_{n+1} = \mathbf{0} \qquad (3)$$

where

$$(\mathbf{f}_A^{\text{int}}) = \begin{bmatrix} \int \mathbf{B}_A^T (\boldsymbol{\sigma}' - n^s p_w \mathbf{1})_{n+1} \, d\Omega_s - \int N_A \boldsymbol{\xi} \cdot (\mathbf{v}_s - \mathbf{v}_w)_{n+1} \, d\Omega_s \\ -\int \mathbf{B}_A^T (n^w p_w \mathbf{1})_{n+1} \, d\Omega_s + \int N_A \boldsymbol{\xi} \cdot (\mathbf{v}_s - \mathbf{v}_w)_{n+1} \, d\Omega_s \end{bmatrix} \qquad (4)$$

$$(\mathbf{f}_A^{\text{ext}}) = \begin{bmatrix} \int N_A \rho^s \mathbf{b}_{n+1} \, d\Omega_s + \int N_A \bar{\mathbf{h}}_{n+1}^s \, d\Gamma_h \\ \int N_A \rho^w \mathbf{b}_{n+1} \, d\Omega_s + \int N_A \bar{\mathbf{h}}_{n+1}^w \, d\Gamma_h \end{bmatrix} \qquad (5)$$

where $\mathbf{B}_A$ represents the nodal strain displacement matrix [$\mathbf{B}_A = \nabla^s N_A(\mathbf{x})$]; N_A denotes the shape function for the Ath node; the quantity $(\mathbf{f}_A^{\text{int}})_{n+1}$ represents the internal forces (both solid and fluid) on node A at time t_{n+1} due to stresses in the soil mass; $(\mathbf{f}_A^{\text{ext}})_{n+1}$ represents the external forces (again, both solid and fluid) applied to node A at time t_{n+1} due to body force and traction-type loads; and $\bar{\mathbf{h}}_{n+1}^s$ and $\bar{\mathbf{h}}_{n+1}^w$ represent the traction vectors per gross unit volume on the solid and fluid phases, respectively. So long as balance can be achieved between the internal soil stresses and external forces, the embankment model will be stable with respect to the applied loads and solutions to the equilibrium equation [(3)] will exist. When this balance can no longer be achieved and equilibrium solutions no longer exist because of finite soil strength and increased gravity loading, the slope model will be unstable and on the verge of failure.

In general, (3) represents a nonlinear algebraic system that must be solved in an iterative fashion for the nodal velocities $\mathbf{v}_{n+1}$ at the $(n + 1)$th step. Upon having realized equilibrium values of $\mathbf{v}_{n+1}$ at each time step, nodal displacements $\mathbf{u}_{n+1}$ are updated by means of a generalized midpoint rule algorithm

$$\mathbf{u}_{n+1} = \mathbf{u}_n + (1 - \varsigma)(\Delta t)_n \mathbf{v}_n + \varsigma(\Delta t)_{n+1} \mathbf{v}_{n+1} \qquad (6)$$

where $\varsigma \in [0, 1]$ = constant integration parameter whose value is chosen as unity in the computations presented herein; and $\mathbf{u}_{n+1}$ and $\mathbf{v}_{n+1}$ respectively denote the displacement and velocity fields at time t_{n+1}.

Nonlinear FEM Equation Solving

The system of nonlinear FEM equilibrium equations to be solved at some time $t_{n+1} \in [0, \infty)$ of the stability analysis problem has the abbreviated form

$$\mathbf{r}_{n+1}(\mathbf{v}_{n+1}) = \mathbf{0} \qquad (7)$$

In the proposed embankment stability analysis method, it is imperative that solutions to (7) be reliably found if and when they exist. For a given time step, the employment of Newton's method in tandem with line searching yields (Fig. 1) a sequence of the global velocity vectors $\mathbf{v}_{n+1}^k$ ($k = 0, 1, \ldots$), which eventually solves the system of (7) when solutions actually exist. In Fig. 1, $\mathbf{K}$ is the global tangent stiffness matrix and s is a scalar line search parameter chosen to satisfy the standard line search criterion (Gerardin and Hogge 1987)
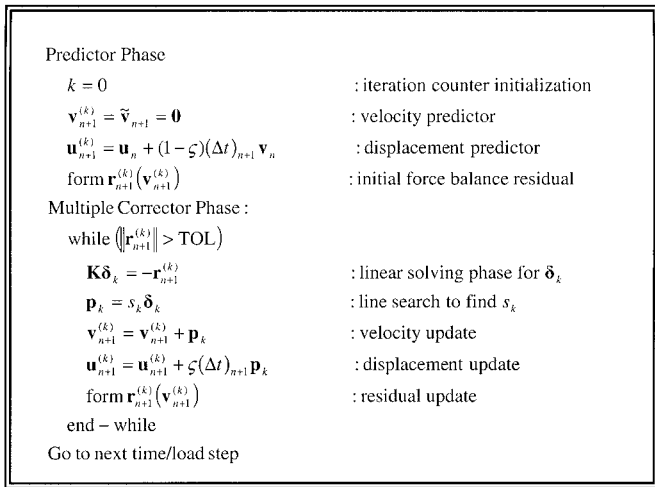
```
Predictor Phase
    k = 0                                    : iteration counter initialization
    v_{n+1}^{(k)} = ṽ_{n+1} = 0              : velocity predictor
    u_{n+1}^{(k)} = u_n + (1 - ς)(Δt)_{n+1} v_n   : displacement predictor
    form r_{n+1}^{(k)}(v_{n+1}^{(k)})        : initial force balance residual
Multiple Corrector Phase :
    while (‖r_{n+1}^{(k)}‖ > TOL)
        Kδ_k = -r_{n+1}^{(k)}                : linear solving phase for δ_k
        p_k = s_k δ_k                        : line search to find s_k
        v_{n+1}^{(k)} = v_{n+1}^{(k)} + p_k  : velocity update
        u_{n+1}^{(k)} = u_{n+1}^{(k)} + ς(Δt)_{n+1} p_k   : displacement update
        form r_{n+1}^{(k)}(v_{n+1}^{(k)})    : residual update
    end - while
    Go to next time/load step
```

FIG. 1. Global Newton-Raphson Solution Algorithm for Typical $(n + 1)$th Time Step

$$\left| \boldsymbol{\delta}_k \cdot \mathbf{r}^{(k+1)}(\mathbf{v}_{n+1}^{(k)} + s_k \boldsymbol{\delta}_k) \right| < \text{STOL} \qquad (8)$$

in which $\boldsymbol{\delta}_k$ = incremental search direction in displacement space; and *STOL* = tolerance parameter controlling the accuracy of the search. In the linear solving phase of Fig. 1, $\mathbf{K} = d\mathbf{r}/d\mathbf{v}$ can be updated each iteration (pure Newton) or updated only periodically (modified Newton).

Modified Predictors for Accelerated Convergence

The proposed solution algorithm in Fig. 1 represents a standard method that would be used in solving nonlinear finite-element equations for a soil system undergoing an arbitrary loading and unloading program. In the proposed stability analysis framework, however, the embankment systems are subjected only to monotonically increasing loading behavior. For such special loading conditions, the displacement and velocity predictors of Fig. 1 can be modified to achieve accelerated convergence in solving the nonlinear finite-element equations. Specifically, the recommended displacement and velocity predictors for use in porous medium limit-state analysis problems are

$$\tilde{\mathbf{u}}_{n+1} = \mathbf{u}_n + (\mathbf{u}_n - \mathbf{u}_{n-1}) \cdot \frac{\|\Delta \mathbf{f}_{n+1}^{\text{ext}}\|}{\|\Delta \mathbf{f}_n^{\text{ext}}\|} \qquad (9a)$$

$$\tilde{\mathbf{v}}_{n+1} = \frac{1}{\varsigma \Delta t_{n+1}} [\tilde{\mathbf{u}}_{n+1} - \mathbf{u}_n - (1 - \varsigma)\Delta t_{n+1} \mathbf{v}_n] \qquad (9b)$$

in which $\Delta \mathbf{f}_{n+1}^{\text{ext}} = \mathbf{f}_{n+1}^{\text{ext}} - \mathbf{f}^{\text{ext}}$. These predictors lead to accelerated convergence, because they essentially use the converged incremental displacements from the preceding load step to estimate (or predict) the incremental displacements over the current load step. The velocity predictor of (9b) is generated by enforcing consistency with the generalized midpoint rule algorithm expressed in (6).

Load-Based Embankment Stability Analysis

In the present slope stability analysis framework, the objective is to hold the gravity loading on the foundation soils fixed while monotonically increasing the gravitational loading applied to the embankment soil mass at a physically meaningful rate. At some point, the slope system becomes unstable and equilibrium solutions to (3) no longer exist [Fig. 2(a)]. As the magnitude of the gravity load vector applied to the embankment $[\mathbf{b}(t)]_{\text{embankment}}$ is increased, the magnitudes of the applied external forces $\mathbf{f}^{\text{ext}}$ [(5)] increase proportionately until the soil mass reaches the limit of its resistive capacity (or strength) and is on the verge of unstable failure. Consistent with Drucker's criterion for material stability, a soil structure that is stable will have a positive definite tangent stiffness matrix $\mathbf{K}$ such that for any kinematically admissible nonvanishing incremental displacement field $\dot{\mathbf{u}}$

$$\dot{\mathbf{u}} \cdot \mathbf{K} \cdot \dot{\mathbf{u}} > 0 \qquad (10)$$

However, as increasing gravity loads are applied to the embankment system, it typically develops an inability to further resist incremental loadings because of the finite shear strengths of its soils. At this point, which is the stability limit of the soil structure, the tangent stiffness operator $\mathbf{K}$ of the soil model becomes positive semidefinite, such that there exists an incremental displacement field $\dot{\mathbf{u}}_{\text{mech}}$ satisfying

$$\Lambda = 0 = \dot{\mathbf{u}}_{\text{mech}} \cdot \mathbf{K} \cdot \dot{\mathbf{u}}_{\text{mech}} \qquad (11a)$$

$$\Lambda = \dot{\mathbf{f}}^{\text{ext}} \cdot \mathbf{K}^{-1} \cdot \dot{\mathbf{f}}^{\text{ext}} \qquad (11b)$$
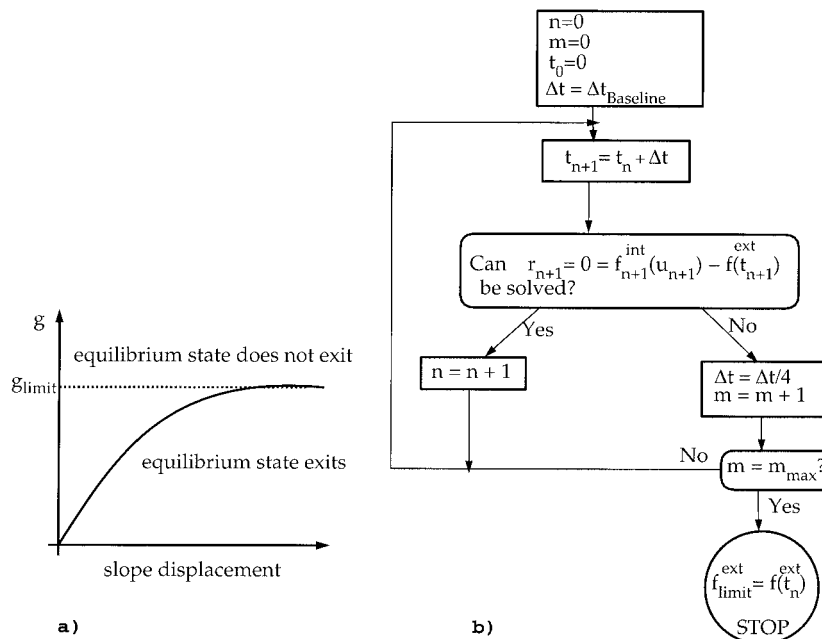

FIG. 2. (a) Limiting Gravity Load at which Slope Failure Occurs; (b) Automated Limit-State Analysis Algorithm

in which, mathematically, $\dot{\mathbf{u}}_{\mathrm{mech}}$ = vector in the null space of $\mathbf{K}$ at the limit of stability. Physically, it represents the incremental motion of the soil structure associated with the failure mechanism(s) developed. If (11b) is normalized by the squared magnitude of incremental external forces, then

$$\lim_{b \to b_{\mathrm{limit}}} \frac{\Lambda}{\dot{\mathbf{f}}^{\mathrm{ext}} \cdot \dot{\mathbf{f}}^{\mathrm{ext}}} = \frac{\dot{\mathbf{f}}^{\mathrm{ext}} \cdot \mathbf{K}^{-1} \cdot \dot{\mathbf{f}}^{\mathrm{ext}}}{\dot{\mathbf{f}}^{\mathrm{ext}} \cdot \dot{\mathbf{f}}^{\mathrm{ext}}} \qquad (12a)$$

$$\lim_{b \to b_{\mathrm{limit}}} \frac{\Lambda}{\dot{\mathbf{f}}^{\mathrm{ext}} \cdot \dot{\mathbf{f}}^{\mathrm{ext}}} = \mathbf{n}^{\mathrm{ext}} \cdot \mathbf{K}^{-1} \cdot \mathbf{n}^{\mathrm{ext}} \qquad (12b)$$

$$\lim_{b \to b_{\mathrm{limit}}} \frac{\Lambda}{\dot{\mathbf{f}}^{\mathrm{ext}} \cdot \dot{\mathbf{f}}^{\mathrm{ext}}} = \infty \qquad (12c)$$

where $\mathbf{n}^{\mathrm{ext}} = \dot{\mathbf{f}}^{\mathrm{ext}}/\|\dot{\mathbf{f}}^{\mathrm{ext}}\|$ = unit vector in the direction of the applied incremental forces. The physical interpretation underlying (12) is that, as the limit of stability is approached for a given magnitude of incremental applied loads, the incremental compliance of the system tends toward infinity.

To avoid the necessity of manual intervention in the stability analysis problem, a reliable and automated solution algorithm is employed. In the proposed algorithm [Fig. 2(b)], a linearly increasing gravitational acceleration vector is applied to the embankment soil mass in time as follows:

$$[\mathbf{b}(t)]_{\mathrm{embankment}} = \dot{\mathbf{b}}_{\mathrm{embankment}} \times t, \quad t \in [0, \infty) \qquad (13)$$

where $\dot{\mathbf{b}}_{\mathrm{embankment}}$ = prescribed vector specifying the direction and rate at which gravity loading is applied to the embankment soil mass; and t = analysis problem's time variable, which assumes a value of zero at the onset of embankment loading. Clearly, $\dot{\mathbf{b}}_{\mathrm{embankment}}$ can be specified to model a desired or trial rate of construction for an embankment. By prescribing the applied gravitational acceleration vector $\mathbf{b}(t)$ in this manner, the stability analysis problem reduces to algorithmically finding the largest time t_{limit} for which a global equilibrium solution of (3) exists. The limiting gravitational acceleration on the embankment system is then merely

$$\mathbf{b}_{\mathrm{embankment}}^{\mathrm{limit}} = \dot{\mathbf{b}}_{\mathrm{embankment}} \times t_{\mathrm{limit}} \qquad (14)$$

Thus, the algorithm of Fig. 2(b) is merely one in which the time t_{limit}, which is not known a priori, is approached asymptotically. For values $t > t_{\mathrm{limit}}$, equilibrium solutions will not exist. Thus if during the $(n + 1)$th time step, the robust solution algorithm of Fig. 1 fails to find a solution for (3), it can be reasonably assumed that an equilibrium solution does not exist and that $t_{n+1} > t_{\mathrm{limit}}$. In this case, the time step Δt_{n+1} is reduced by a factor of p and the algorithm reverts to time t_n, which is the most recent (or largest) time for which an equilibrium solution exists. In the algorithm of Fig. 2(b), the parameter m_{max} is typically set to a value between 10 and 20, with larger values leading to more precise satisfaction of the limit-state conditions of (11) and (12) and thus more accurate computation of $\|\mathbf{b}_{\mathrm{embankment}}^{\mathrm{limit}}\|$. At a given problem time t, failure to find a solution could also result from lack of a robust nonlinear equation-solving algorithm.

There are a number of potential indicators for gauging the reliability of the nonlinear equation-solving algorithm. If the solution algorithm of Fig. 1 fails to find a solution, the time step is reduced by a factor of p, and the solution method then succeeds in finding a solution for $>p$ successive steps, it indicates that the prior failure to find a solution was due to lack of robustness in the solving algorithm rather than the lack of a solution. Therefore, whenever a limit has been found by the algorithm of Fig. 2b, the criterion of (12) should be checked to verify that a true limit has indeed been found.

In accordance with the fact that embankment construction

is here the active agent that induces failure of the system, the proposed load-based factor of safety against embankment failure is simply

$$(\mathrm{FS})_{\mathrm{load}} \equiv \frac{\|\mathbf{b}\|_{\mathrm{embankment}}^{\mathrm{limit}}}{\|\mathbf{b}\|_{\mathrm{actual}}} \qquad (15)$$

in which $\|\mathbf{b}\|_{\mathrm{actual}}$ = appropriate and representative actual gravitational acceleration for the embankment being analyzed (i.e., $\|\mathbf{b}\|_{\mathrm{actual}} \cong 9.81$ m/s^2 $\cong 32.2$ ft/s^2). In general, the computed $(FS)_{\mathrm{load}}$ will be dependent upon the rate at which the embankment is constructed. The higher the computed factor of safety is for a given embankment and rate of construction, the more stable that system is against failure. Computed values of $(FS)_{\mathrm{load}}$ that are less than unity indicate an unstable embankment system for the given rate of construction, and values equal to or larger than unity indicate a stable system.

Application of Loads to Soil Mass

The field shear strength behavior of most soils is strongly dependent upon the in situ state of effective normal stresses. Consequently, careful attention must usually be paid to both the manner and the order in which gravitational loads are applied to embankment models. For example, a totally unstressed, cohesionless soil, whose shear strength is governed by either Mohr-Coulomb or Drucker-Prager models, is on the verge of shear failure when in a fully unstressed state. The same would not be true, however, for an overconsolidated soil with a significant initial cohesion. For most noncohesive soils, it is thus important to first apply appropriate and realistic confining stresses to the slope models before shearing loads associated with slopes are applied (Seo 1998). If the soil models are not prestressed in the manner described, they may not feature realistic strength behaviors and the predicted stability of the embankment system will be unrealistically low. For the special case of soils with substantial initial cohesion, however, the order of loading is typically unimportant.

Applying these principles to the problem at hand within the proposed framework, gravity loading is first applied to the soft saturated foundation soils and they are then permitted to achieve a normally consolidated equilibrium state. If the foundation soils on which the embankment is to be constructed are initially overconsolidated, applying a surcharge load to the soil model for a given duration and then releasing it can capture this effect. This pretreatment gives the foundation soils in the numerical model a realistic initial state of effective stresses that define the soil's mechanical condition in terms of both shear strength and compressibility. Shear strength and compressibility effects can be realistically modeled with the elastoplastic cap models discussed below.

Once the foundation soils in the numerical model are in an equilibrium condition consistent with an appropriate preloading program, the gravity loading acting upon them is held fixed for the remainder of the problem at the value $\mathbf{b}_{\mathrm{actual}}$. The next stage of the analysis involves gradually increasing the gravity loading on the embankment system in accordance with (13), up to the point where an unstable failure mechanism has fully developed. During this stage of the analysis, the development of excess pore pressures in the foundation soil are modeled along with coupled distortional and volumetric elastoplastic deformation.

It is emphasized that in the approach being proposed here, a fixed and realistic gravity loading is applied to the foundation soils while the gravity loading on the embankment system is gradually increased. If gravity loading applied to the foundation soils were instead further increased along with the gravity loading applied to the embankment, this would have the effect of further increasing the modeled shear strength of the

foundation soils and this in turn would result in larger computed factors of safety against instability. This would be both unrealistic and unconservative, because physically, the gravitational loading on the foundation soils does not change during embankment construction. Hence, applying a monotonically increasing gravity loading only to the embankment soil and not the foundation soil is both more realistic and more conservative.

MATERIAL MODEL REQUIREMENTS

The proposed slope stability analysis method can, in principle, be applied with a wide variety of soil plasticity models. The method will generally provide more useful results and converge more rapidly, however, when realistic soil models are used that feature continuous and smooth differentiability of the rate constitutive equations.

To efficiently model coupling between tensile, compressive, and shearing modes of ductile soil plasticity, a smooth, three-surface cap model (Fig. 3) is employed in the calculations presented in the following section. The model employed here is a smooth variation of the nonsmooth cap model originally proposed by DiMaggio and Sandler (1971) and developed for FEM implementation by Simo et al. (1988). This soil plasticity model was implemented (Swan and Seo 2000) with a fully implicit integration algorithm and consistent material tangent operators (Simo and Hughes 1998). For completeness, the basic constitutive equations, yield functions, flow rules, and hardening laws associated with this model are presented in the Appendix.

Because the Mohr-Coulomb yield criterion has a long history of use in classical soil mechanics, geotechnical engineers often think of soil shear strength characteristics in terms of the Mohr-Coulomb cohesion c and friction angle ϕ. Here, the nonlinear Drucker-Prager failure envelope with tension and compression caps and with saturating frictional effects is employed because

- It captures the saturation of soil strength with increasing effective confining stresses.
- It is a completely smooth model having no corner regions. The Drucker-Prager model does not suffer from the nonsmooth corner regions that generally afflict Mohr-Coulomb–type soil models (Zienkiewicz 1975).

So that the results of the present work can be compared with results of classical slope-stability analysis methods wherein the Mohr-Coulomb failure criterion is routinely considered, the yield criterion in (23) and (26) is rewritten by taking its Taylor's series expansion about $I_1 = 0$

$$f(\boldsymbol{\sigma}) = \|\mathbf{s}\| - \left\{ \alpha - \theta I_1 \left[1 + \frac{\beta I_1}{2} + \frac{(\beta I_1)^2}{6} + \frac{(\beta I_1)^3}{24} + \cdots \right] \right\} \quad (16)$$

where $\mathbf{s}$ = deviatoric stress tensor; $I_1 = (\sigma_{11} + \sigma_{22} + \sigma_{33})$; and $\theta \equiv \lambda\beta$ = slope of the envelope at $I_1 = 0$. For small values of I_1 (i.e., $\beta I_1 \ll 1$), the linearized form of the yield function is

$$f(\boldsymbol{\sigma}) = \|\mathbf{s}\| - \{\alpha - \theta I_1\} \quad (17)$$

which is simply a variation of the linear Drucker-Prager yield criterion. A correspondence can be established between the two parameters α and θ of the linearized Drucker-Prager envelope of (17) and the cohesion c and friction angle ϕ of the Mohr-Coulomb envelope. Translations from Mohr-Coulomb parameters to linear Drucker-Prager parameters have been provided, for example, by Chen and Saleeb (1982)

$$\alpha = \frac{\sqrt{2}c}{\left(1 + \frac{4}{3}\tan^2\phi\right)^{1/2}}; \quad \theta = \frac{\sqrt{2}\tan\phi}{3\left(1 + \frac{4}{3}\tan^2\phi\right)^{1/2}} \quad (18)$$
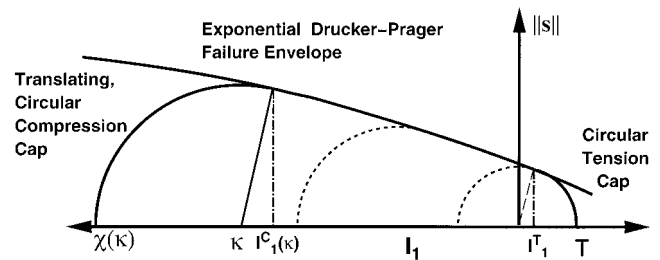

FIG. 3. Three-Surface, Two-Invariant Cap Plasticity Model Used in Embankment Stability Analysis Computations

These equations can be inverted to provide a translation from linear Drucker-Prager envelope parameters to Mohr-Coulomb, which will be used in the following section:

$$c = \frac{\alpha}{\sqrt{2}}\left(1 + \frac{4}{3}\tan^2\phi\right)^{1/2}; \quad \tan\phi = \frac{3\theta}{\sqrt{2}\sqrt{1 - 6\theta^2}} \quad (19)$$
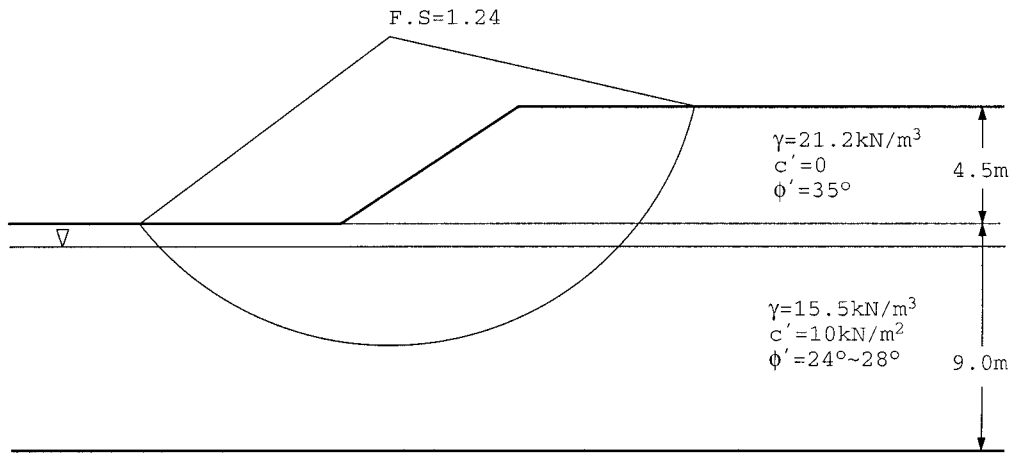
EMBANKMENT STABILITY COMPUTATIONS

A sand embankment was built for experimental purposes at Cubzac-les-Point, France, in 1971. The experimental test program included the fairly rapid 10-day construction of an embankment on a soft, saturated clay stratum, up to a height of 4.5 m and slope angle of 34°, at which point an instability mechanism developed. Here, this experiment is revisited with the proposed computational method to analyze the embankment's stability for a number of different rates of construction both with and without use of sand drains. The results are in general agreement with the Cubzac-les-Point experimental result and also quantify the short-term stabilizing influence of sand drains.

Cubzac-les-Point Embankment

In 1982, Pilot et al. (1982) analyzed the Cubzac embankment using both effective and total stress analyses with Bishop's simplified method of slices. In their analysis, the foundation consisted of soft silty clay having an approximate thickness of 9 m. The effective Mohr-Coulomb (drained) shear strength parameters measured in triaxial compression tests were $c' = 10$ kPa and ϕ' between 24° and 28°. (In the sample computations in this paper, the friction angle of the soft silty clay was taken as 26°.) The water table was taken to coincide roughly with the ground level. The embankment material was a clean gravelly sand with an in situ density of 21 kN/m³; its Mohr-Coulomb shear strength parameters were estimated to be $c' = 0$ kPa and $\phi' = 35°$. Fig. 4 shows a schematic of the test embankment, material properties, and computed failure mechanism of Pilot et al. (1982) having an associated resistance safety factor of 1.24.

In the test computations in this paper, the foundation is modeled as a saturated clayey soil having a thickness of 9 m, which has been normally consolidated by applying gravitational loading and allowing the soil to achieve a fully drained equilibrium. The shear and compressive behavior of the clay soil is modeled with the elastoplastic cap model described in the previous section and the Appendix. A reasonable value for the Drucker-Prager parameter $\beta = 10^{-7}$ Pa^{-1} was assumed for the clay soil, and the other two Drucker-Prager envelope factors (α and λ) were computed from the Mohr-Coulomb values listed above and from (18) and (19). The compressibility characteristics of the clay soil at the Cubzac-les-Point site were not reported, making it necessary to estimate reasonable compressibility behaviors. This can be done by assuming reasonable values of such quantities as the liquid limit, the initial void ratio e_0, the initial water content w_0, and the specific grav-

FIG. 4. Cross Section of Cubzac Embankment with Failure Mechanism and Safety Factor Computed by Pilot Using Classical Methods of Slope Stability Analysis

TABLE 1. Material Parameters Used for Embankment Computations

Parameter	Foundation soil	Embankment soil
ρ^s	1,600 kg/m³	2,161 kg/m³
μ	208.3 MPa	1.154 GPa
E	500 MPa	3.0 GPa
κ_0	0.0 kPa	—
α	12.3 kPa	10.0 Pa
λ	400.6 kPa	153 kPa
β	(2.0 MPa)$^{-1}$	(0.575 MPa)$^{-1}$
D	(3.125 MPa)$^{-1}$	—
W	0.15	—

ity G_s, of the grains in the soft clay soil. From such reasonable estimates, the standard compression index C_c for the soil can be estimated using a wide variety of empirical relations summarized in Das (1998). The compression index was then used to estimate the cap model compressibility parameters W and D of the cap model, as listed in Table 1, following Huang and Chen (1990). The permeability of the clay soil was also not measured, so a reasonable estimate characteristic of that for silty clay soils (Das 1998) was assumed ($k_c = 8.6 \cdot 10^{-5}$ m/day).

The 4.5-m embankment was modeled as a dry sandy soil using a Drucker-Prager model and a tension cap with no compression cap, because compressibility effects in the sand were judged to be of minor importance. Only the friction angle of the embankment sand was reported by Pilot et al. (1982). It is noted, however, that the proposed stability analysis techniques typically require a yield surface with an ultimate limit (or saturation) of frictional shear strength. A sand with an initial friction angle of 35° was used, and the sand shear strength experiments of Desai et al. (1981) were used to estimate a reasonable shape of the Drucker-Prager yield surface featuring saturation of frictional strengthening effects. Recalling that θ = λβ and also (18), which relates θ to the Mohr-Coulomb friction angle ϕ', the λ and β values were selected as shown in Table 1.

Construction was simulated by gradually increasing gravity loading on the embankment soil until critical failure mechanisms developed. The critical load factors were computed using the stability analysis techniques described above. As gravity loading on the embankment was gradually increased, gravity loading applied to the base soil was held constant. The computed load-based safety factors and failure mechanisms for different rates of construction are shown in Fig. 5 and clearly demonstrate that stability increases with more gradual construction. It should be noted that our computed 10-day load-based factor of safety for this embankment is 0.922, whereas Pilot et al. (1982) predicted a resistance safety factor of 1.24,

which would imply a marginally stable embankment. It is emphasized that, in the models in this paper, reasonable estimates for soil properties were used where data were lacking. In selecting soil parameter values, no effort was made to tune these model results to fit the Cubzac-les-Point result.
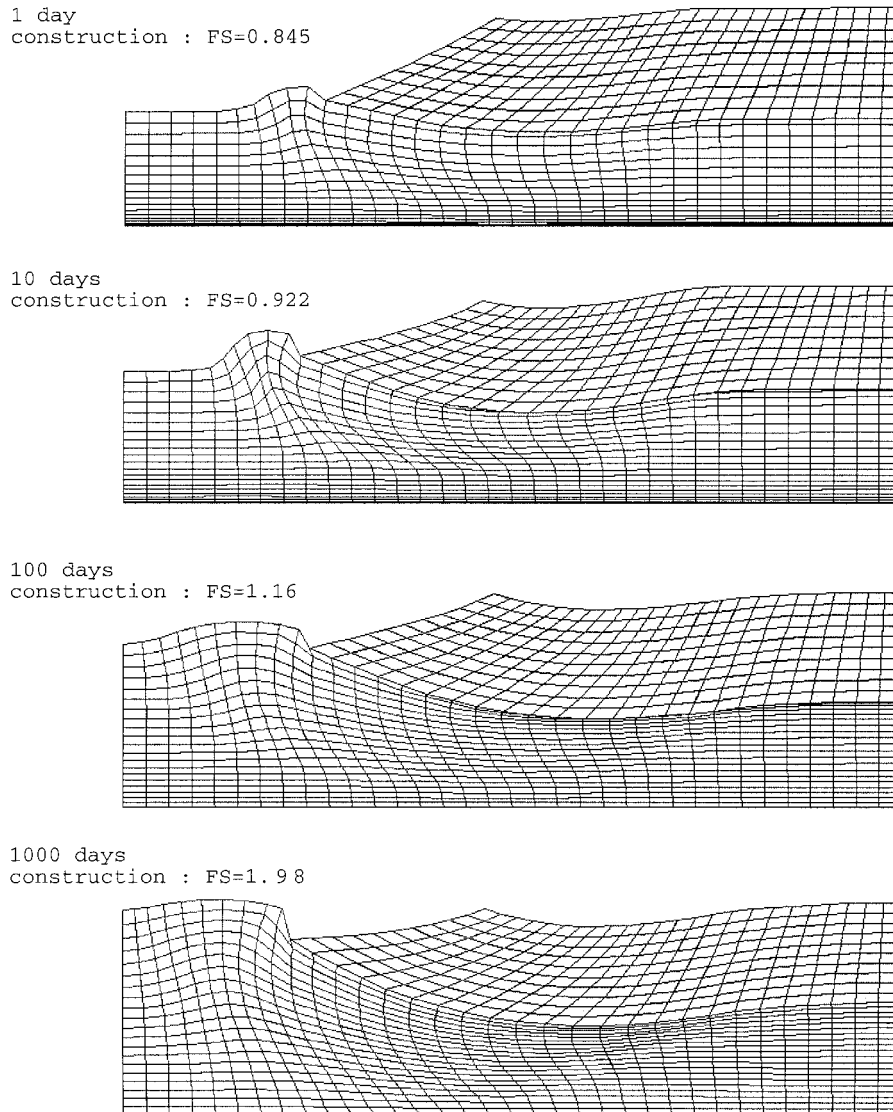
Cubzac-les-Point Embankment with Sand Drains

The use of sand drains is one of many available soil improvement techniques used to hasten consolidation of soft, saturated soil deposits. Sand drains are constructed by excavating shafts in the soft native soil and then backfilling them with sand. Such drains facilitate more rapid dissipation of pore pressures when the surcharge loads are applied; thus, they permit more rapid construction of embankments. In computing embankment stabilities with sand drains, the preconsolidation of the soft clay foundation soil was done as in the previous example. The material properties of the soil in the drains were then changed from those of clay to those of sand, and the soils were allowed to re-equilibrate. Gravitational loading was then applied to the embankment until instabilities were detected. Although the clay was modeled with permeability of $k_c = 8.6 \cdot 10^{-5}$ m/day, the sand was modeled with an assumed $k_s = 1,000k_c$. (Note: These results are insensitive to the actual permeability of the sand, because the permeability of the clay determines the time it takes pore water to reach the drains.) The computed factors of safety with sand drains and the deformed embankment shapes at failure are shown in Fig. 6.

A comparison of computed embankment stability factors versus construction time, both with and without sand drains, is shown in Fig. 7. These results demonstrate the significant variation in stability of an embankment with rate of construction. The stability factors for very rapid construction rates, which lead to undrained behavior of the foundation soil, and very slow construction, which permits complete drainage of the foundation soil, differ by a factor of approximately 4. The method also predicts that use of sand drains, with the spacing modeled, would allow the embankment to be safely constructed on a timescale of 1–10 days.

DISCUSSION OF METHODS AND RESULTS

The examples above demonstrate the viability and utility of the proposed embankment stability analysis techniques. The attractive aspect of these techniques is that they permit the analyst to quickly consider a number of embankment construction rates and to identify those that will be both timely and safe. The method of modeling the gradual construction of the embankment, by steadily increasing the gravity loading acting upon it at a prescribed rate, is an approximation requiring very

1 day
construction : FS=0.845

10 days
construction : FS=0.922

100 days
construction : FS=1.16

1000 days
construction : FS=1.98

FIG. 5. Computed Failure Mechanisms and Safety Factors for Different Rates of Embankment Construction

little human interaction. Once a suitable rate of construction is identified with these techniques, one can then perform more traditional step-by-step analysis of the embankment construction sequence using more labor-intensive techniques (Huang et al. 1992) to confirm the results of this analysis.

It is reemphasized that the techniques proposed here differ from those used in resistance-based stability analysis, which is much more commonly used in geotechnical engineering. Whereas resistance-based safety factors and stability analysis can be used with standard Mohr-Coulomb soil models, load-based stability analysis can only be guaranteed to produce meaningful factors of safety when the soil models used feature a saturation of frictional strengthening effects. In this sense, load-based stability analysis techniques require more realistic soil models than do resistance-based techniques.

Although not implemented and tested here, there are a number of possibilities by which the proposed analysis techniques could be modified and applied within a strength-reduction stability analysis framework. As one example, the resistance-based stability of an embankment at a trial rate of construction could be assessed by gradually applying the gravity loading to the embankment at the desired rate up to $\mathbf{b}_{embankment} = \mathbf{b}_{actual}$. At the completion of construction, the pore-pressure field in the soils could be held fixed while the shear strengths of the foundation and embankment soils would be instantaneously

reduced by a sufficient amount to induce instability of the system. The factor by which the strengths of the soils would need to be reduced to create instability would constitute the resistance-based factor of safety for the selected rate of construction. This is but one variation that can be tested in future efforts.

SUMMARY AND CLOSURE

Both load and resistance factor slope stability methods can be used to assess the stability of embankments. In the load-factor approach presented here, the loading is applied to the embankment at a rate that simulates the planned rate of construction. To account for critical pore-pressure diffusion effects, the saturated foundation soil was modeled with porous medium theory and an elastoplastic cap model that allows the stability analysis to capture the coupling between the soil's compressibility (consolidation) and shear strength behaviors. In the demonstrative example, an embankment corresponding to a field test experiment (with an actual construction rate of 10 days) was modeled. The proposed analysis framework predicts a stability factor of safety (0.92) that is in general agreement with the observed failure in the Cubzac-les-Point field test. Going beyond the Cubzac-les-Point case study, the proposed method was also exercised to compute load stability
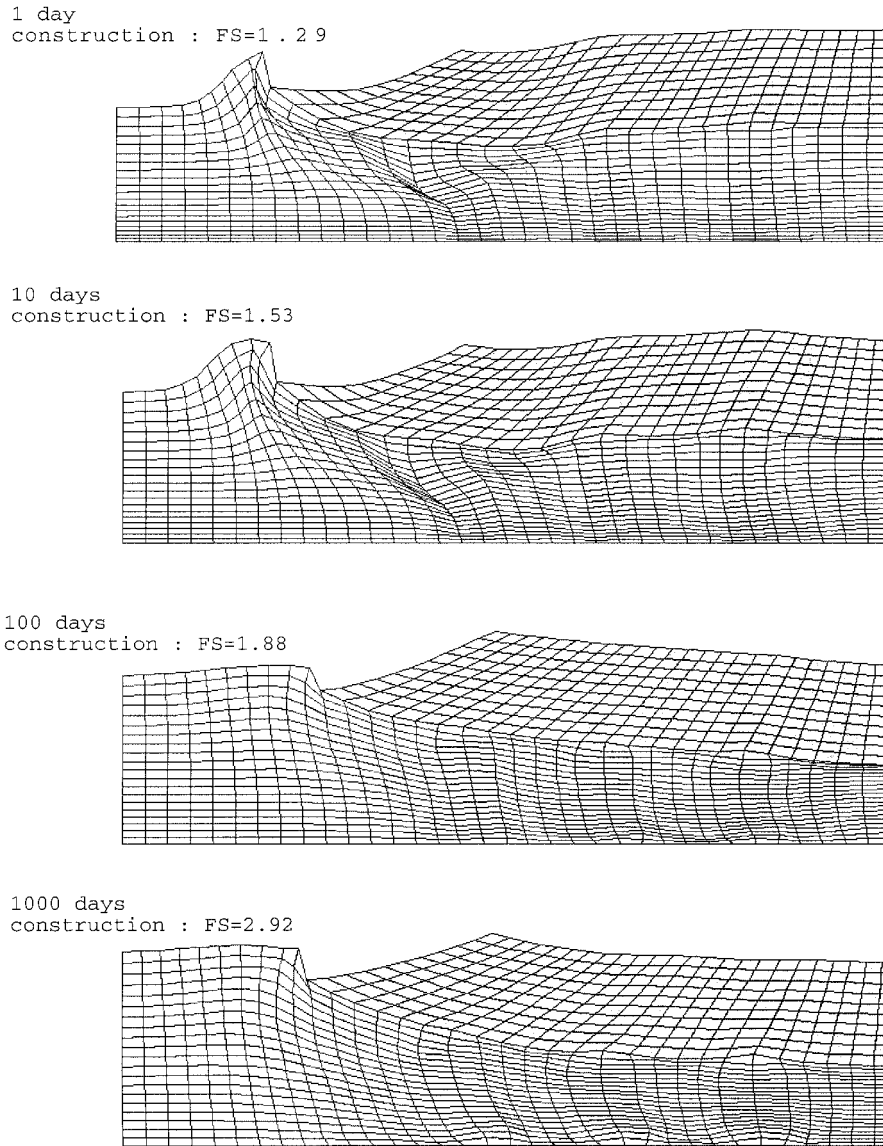
1 day
construction : FS=1.29

10 days
construction : FS=1.53

100 days
construction : FS=1.88

1000 days
construction : FS=2.92

FIG. 6. Computed Failure Mechanisms and Safety Factors for Different Rates of Embankment Construction, with Sand Drains

factors for a number of different construction rates, ranging from 0.1 to 10,000 days, and also with use of sand drains. The perceived utility of the proposed method is that it facilitates stability analysis of embankments as a function of construction rate by taking into account the in situ soil stresses, soil shear strength, and transient effects of pore-pressure diffusion.

APPENDIX. SMOOTH CAP MODEL DESCRIPTION

For simplicity, the rate form of this model is described here in a small deformation framework. Although in soil mechanics, compressive stresses are typically assigned positive values, in this explanation, a conventional continuum mechanics sign convention is used, making tensile stresses and strains positive.

The small strain tensor admits the additive elastic-plastic decomposition

$$\boldsymbol{\varepsilon} = \boldsymbol{\varepsilon}^e + \boldsymbol{\varepsilon}^p \qquad (20)$$

where $\boldsymbol{\varepsilon}$, $\boldsymbol{\varepsilon}^e$, and $\boldsymbol{\varepsilon}^p$ = total, elastic, and plastic strain tensors, respectively. The small deformation incremental stress response of the soil skeleton is assumed to be related to the strain response by

$$\dot{\boldsymbol{\sigma}}' = \mathbf{C}:(\dot{\boldsymbol{\varepsilon}} - \dot{\boldsymbol{\varepsilon}}^p) \qquad (21)$$

where $\mathbf{C} = K\mathbf{1} \otimes \mathbf{1} + 2\mu\mathbf{I}_{\text{dev}}$ = fourth-order isotropic tensor of elastic moduli, in which K = bulk modulus of the soil and μ = shear modulus. (The notation employed here follows that of classical continuum mechanics.)

In effective stress space, the elastic domain is bounded by three distinct but smoothly intersecting yield surfaces, as shown in Fig. 3. Surface 1 is called a Drucker-Prager failure envelope, surface 2 is the translating growing/shrinking compression cap, and surface 3 is the stationary tension cap. The mathematical forms of the individual yield functions, $f_k(\boldsymbol{\sigma}, \kappa)$ ($k = 1, 2,$ or 3) are

$$f_1(\boldsymbol{\sigma}) = \|\mathbf{s}\| - F_e(I_1) \le 0 \qquad (22)$$

$$f_2(\boldsymbol{\sigma}, \kappa) = \|\mathbf{s}\|^2 - F_c(I_1, \kappa) \le 0 \qquad (23)$$

$$f_3(\boldsymbol{\sigma}) = \|\mathbf{s}\|^2 - F_t(I_1) \le 0 \qquad (24)$$

where $\mathbf{s}$ = deviatoric stress tensor and $\|\mathbf{s}\|^2 = (1/2)J_2 = \sqrt{s_{ij}s_{ij}}$; $I_1 = \text{tr}(\boldsymbol{\sigma}')$ = first invariant of the effective stress tensor $\boldsymbol{\sigma}'$; κ = internal hardening variable governing the location of the compressive cap surface (and related to the preconsolidation stress of the soil); and the functional forms of the envelope functions F_e, F_c, and F_t describing the Drucker-Prager surface, compression cap, and tension cap are simply

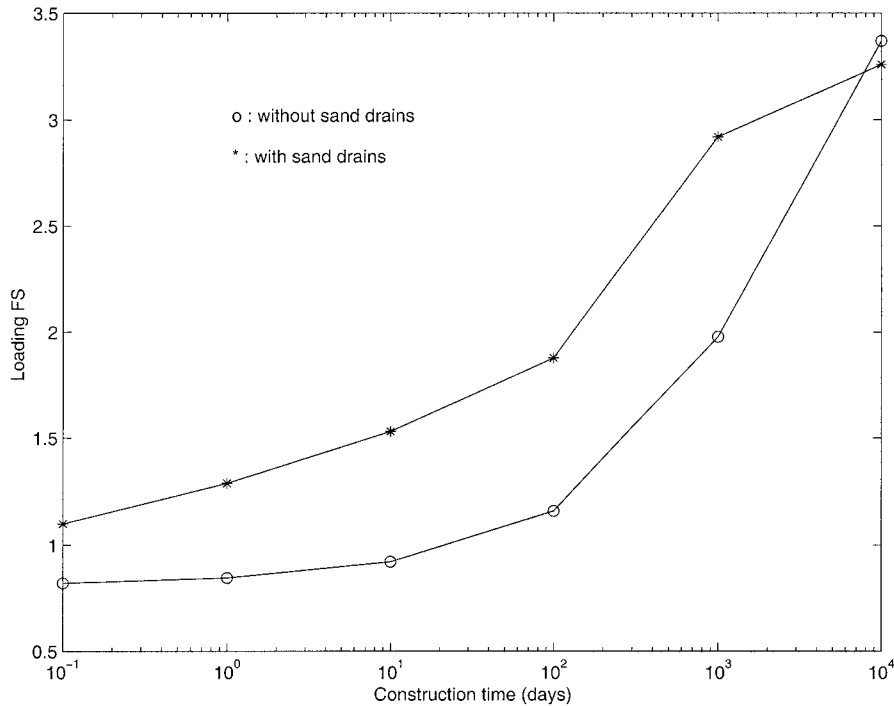$$F_e(I_1) = \alpha + \{1 - \exp(\beta I_1)\}, \quad I_1^C(\kappa) \le I_1 \le I_1^T \qquad (25)$$

FIG. 7. Computed Safety Factors versus Construction Duration for Cubzac-les-Point Embankment with and without Sand Drains

$$F_c(I_1, \kappa) = F_e^2(\kappa) - R^2(\kappa), \quad I_1 < I_1^C(\kappa) \qquad (26)$$

$$F_t(I_1) = T^2 - I_{1i}^2, \quad I_1 > I_1^T \qquad (27)$$

where the following are material model constants from which all others can be derived: $\alpha \geq 0$, $\lambda \geq 0$, and $\beta \geq 0$. The yield surfaces $f_1 = 0$ and $f_3 = 0$ depend only on the stress invariants I_1 and $\|s\|$ and thus remain fixed in stress space, whereas the compression cap surface is permitted to translate along the I_1 axis, and in particular, moves to the right ($\dot{\kappa} > 0$) during plastic dilatation of the medium and to the left ($\dot{\kappa} < 0$) during plastic compression. As the compression cap translates, its radius $R(\kappa)$ evolves in a manner that maintains smooth tangency between the Drucker-Prager envelope and the compression cap surface. The meaning of parameters I_1^T and $I_1^C(\kappa)$ is shown in Fig. 3. In the function F_e, the constants α, λ, and β can be related to the Mohr-Coulomb angle of friction ϕ and cohesion c as discussed in the article.

The flow rule for this smooth model is associated and of the form

$$\dot{\boldsymbol{\varepsilon}}^p = \sum_k \dot{\gamma}^k \frac{\partial f_k}{\partial \boldsymbol{\sigma}'} \qquad (28)$$

with loading/unloading criteria for each surface f_k ($k = 1, 2,$ or 3) governed by the Karesh-Kuhn-Tucker conditions

$$f_k \leq 0; \quad \dot{\gamma}^k \geq 0; \quad \dot{\gamma}^k f_k = 0 \qquad (29)$$

The generalized plastic consistency condition is expressed

$$\dot{\gamma}^k \dot{f}_k = 0 \qquad (30)$$

In the three preceding expressions, $\dot{\gamma}^k$ denotes the incremental plastic deformation associated with the kth yield surface.

The hardening law for this model derives from the assumption that the plastic volumetric compression behavior (plastic volumetric strain ε_v^p versus I_1) is an exponential of the form

$$\varepsilon_v^p = -W\{1 - \exp[D\chi(\kappa)]\} \qquad (31)$$

where $\chi(\kappa) =$ apex point of the cap surface on the I_1 axis; ε_v^p denotes the plastic volumetric strain in the soil as measured from a virgin, completely unloaded state; W represents the maximum possible plastic volumetric strain for the soil; and $D^{-1} = I_1^{\mathrm{ref}}$ denotes the (absolute) value of I_1 at which $\exp\{-1\} \cdot 100\%$ of the soil's original removable porosity remains. Differentiating (31) with respect to κ permits the introduction of a variable tangent hardening modulus $h'(\kappa)$ for κ as follows:

$$h'(\kappa) = \frac{d\kappa}{d\varepsilon_v^p} = \frac{\exp[-D\chi(\kappa)]}{WD\chi'(\kappa)} \qquad (32)$$

where $\chi'(\kappa) = 1 - R'(\kappa)$. Based on (31) and (32), it is clear that, as $\chi \to -\infty$, $\varepsilon_v^p \to -W$ and $h'(\kappa) \to \infty$. This nonlinear hardening modulus $h'(\kappa)$ is used to provide a nonlinear incremental hardening law governing movement of the cap parameter

$$\dot{\kappa} = h'(\kappa)\mathrm{tr}(\dot{\boldsymbol{\varepsilon}}_v^p) \qquad (33)$$

REFERENCES

Bathe, K. J., Snyder, M. D., Cimento, A. P., and Rolph, W. D. (1980). "On some current procedures and difficulties in finite element analysis of elasto-plastic response." *Comp. and Struct.*, 12, 607–624.

Biot, M. A. (1962). "Mechanics of deformation and acoustic propagation in porous media." *J. Appl. Phys.*, 33, 1482–1489.

Borja, R. I. (1986). "Finite element formulation for transient pore pressure dissipation: A variational approach." *Int. J. Solids and Struct.*, 22, 1201–1211.

Burland, J. B. (1965). "The yielding and dilation of clay." *Géotechnique*, London, 15(2), 211–214.

Chen, W. F., and Mizuno, E. (1990). *Nonlinear analysis in soil mechanics: Theory and implementation*, Elsevier Science, New York.

Chen, W.-F., and Saleeb, A. F. (1982). *Constitutive equations for engineering materials, Vol. 1: Elasticity and modeling*, Wiley, New York.

Das, B. M. (1998). *Principles of geotechnical engineering*, 4th Ed., PWS/KENT Publishing Co., Boston.

Desai, C. S., Phan, H. V., and Sture, S. (1981). "Procedure, selection and application of plasticity models for a soil." *Int. J. Numer. and Analytical Methods in Geomech.*, 4, 295–311.

Desai, C. S., Somasundaram, S., and Frantziskonis, G. (1986). "A hierarchical approach for constitutive modeling of geologic materials." *Int. J. Numer. and Analytical Methods in Geomech.*, 10, 225–257.

DiMaggio, F. L., and Sandler, I. S. (1971). "Material models for granular soils." *J. Engrg. Mech.*, ASCE, 97(3), 935–950.

Farhat, C., Park, K. C., and Yves, D.-P. (1991). "An unconditionally

stable staggered algorithm for transient finite element analysis of coupled thermoelastic problems.'' *Comp. Methods in Appl. Mech. Engrg.*, 85, 349–365.

Gerardin, M., and Hogge, M. (1987). ''Solving systems of nonlinear equations.'' *Finite element handbook*, H. Kardestuncer, ed., McGraw-Hill, New York, 4.64–4.72.

Hofstetter, G., Simo, J. C., and Taylor, R. L. (1993). ''A modified cap model: Closest point solution algorithms.'' *Comp. and Struct.*, 46(2), 203–214.

Huang, T.-K., and Chen, W.-F. (1990). ''Simple procedure for determining cap-plasticity-model parameters.'' *J. Geotech. Engrg.*, ASCE, 116(3), 492–513.

Huang, T. K., Chen, W. F., and Chameau, J. C. (1992). ''The application of cap-plasticity-model to embankment problems.'' *Comp. and Struct.*, 44(6), 1349–1369.

Nash, D. F. T. (1987). ''A comparative review of limit equilibrium methods of stability analysis.'' *Slope stability: Geotechnical engineering and geomorphology*, M. G. Anderson and K. S. Richards, eds., Wiley, New York, 11–75.

Pilot, G., Trak, B., and La Rochelle, P. (1982). ''Effective stress analysis of the stability of embankments on soft soils.'' *Can. Geotech. J.*, Ottawa, 19, 433–450.

Prevost, J. H. (1980). ''Mechanics of continuous porous media.'' *Int. J. Engrg. Sci.*, 18, 787–800.

Prevost, J. H. (1987). ''Dynamics of porous media.'' *Geotechnical modeling and applications*, S. M. Sayed, ed., Gulf Publishing Co., Houston, 77–145.

Prevost, J. H. (1998). ''Partitioned solution procedure for simultaneous integration of coupled-field problems.'' *Communications in Numer. Methods in Engrg.*, 13(4), 239–247.

Roscoe, K. H., Schofield, A. N., and Wroth, C. P. (1958). ''On the yielding of soils.'' *Géotechnique*, London, 8(11), 22–53.

Seo, Y.-K. (1998). ''Computational methods for elasto-plastic slope stability analysis with seepage.'' PhD dissertation, University of Iowa, Iowa City, Iowa.

Simo, J. C., and Hughes, T. J. R. (1998). *Computational inelasticity*, Springer, New York.

Simo, J. C., Ju, J.-W., Pister, K. S., and Taylor, R. L. (1988). ''Assessment of cap model: Consistent return algorithms and rate-dependent extension.'' *J. Engrg. Mech.*, ASCE, 114(2), 191–218.

Smith, I. M., and Hobbs, R. (1976). ''Biot analysis of consolidation beneath embankments.'' *Géotechnique*, London, 26(1), 149–171.

Swan, C. C., and Seo, Y.-K. (1999). ''Limit state analysis of earthen slopes using a continuum/FEM approach.'' *Int. J. Numer. and Analytical Methods Geomech.*, 23, 1359–1371.

Swan, C. C., and Seo, Y.-K. (2000). ''A smooth cap plasticity model for soils: Integration algorithm, parameter estimation and applications.'' *Tech. Rep. No. 2000-043*, Ctr. for Comp.-Aided Des., University of Iowa, Iowa City, Iowa.

Truesdell, C. (1965). *The elements of continuum mechanics*, Springer, New York.

Zienkiewicz, O. C., Humpheson, C., and Lewis, R. W. (1975). ''Associated and non-associated viscoplasticity and plasticity in soil mechanics.'' *Géotechnique*, London, 25, 671–689.

Zienkiewicz, O. C., Paul, D. K., and Chan, A. H. C. (1988). ''Unconditionally stable staggered solution procedure for soil-pore fluid interaction problems.'' *Int. J. Numer. Methods in Engrg.*, 26, 1039–1055.

Zienkiewicz, O. C., and Shiomi, T. (1984). ''Dynamic behavior of saturated porous media: The generalized Biot formulation and its numerical solution.'' *Int. J. Numer. and Analytical Methods Geomech.*, 8, 71–96.